

FIG. 1.

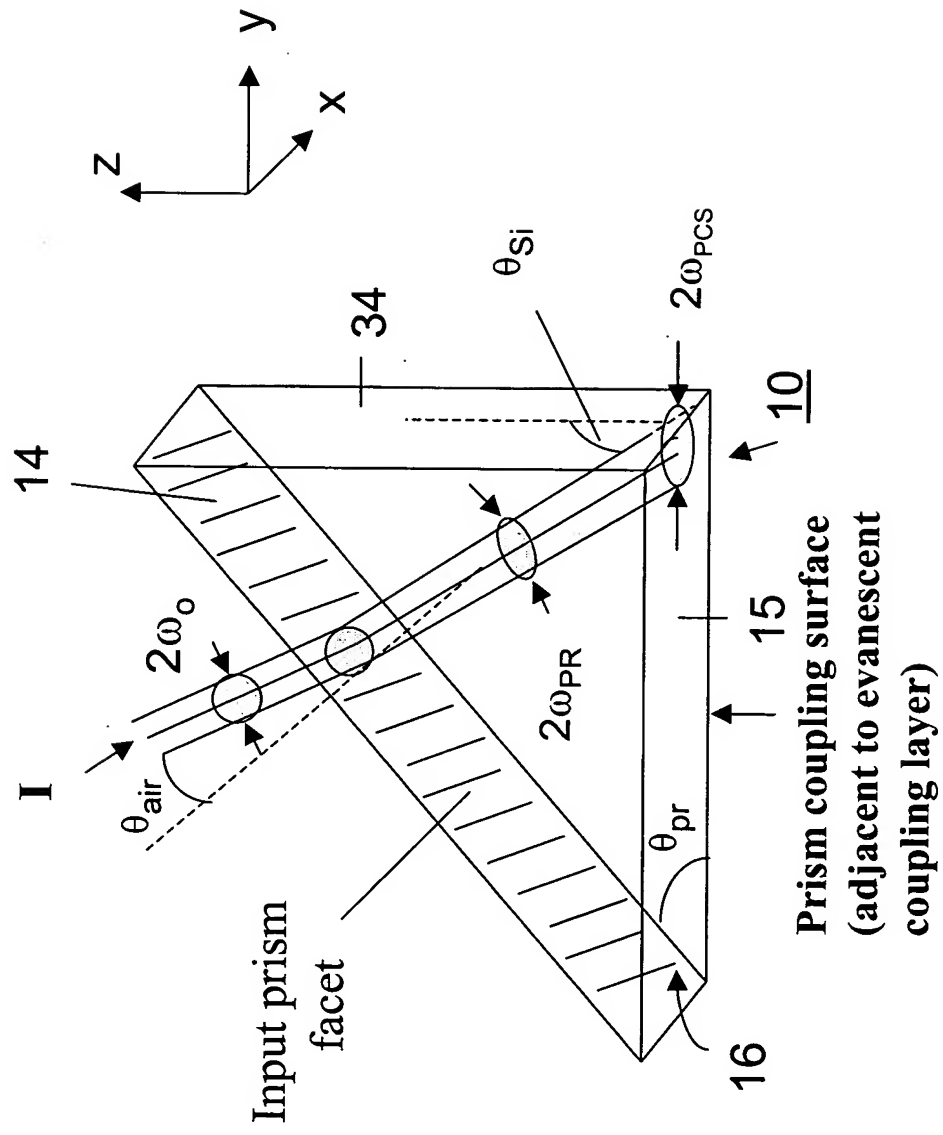


FIG. 2.

Wavelength dependence of beam angle inside prism (θ_{Si}) as a function of wavelength, for three different waveguide thicknesses.

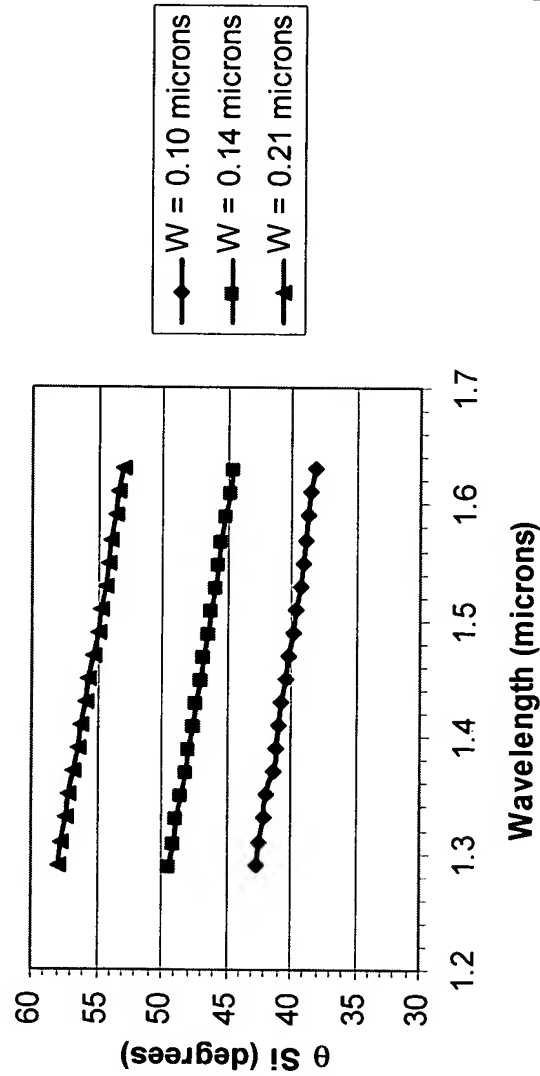


FIG 3.

Wavelength dependence of beam angle in air (θ air) as a function of wavelength, for three different waveguide thicknesses.

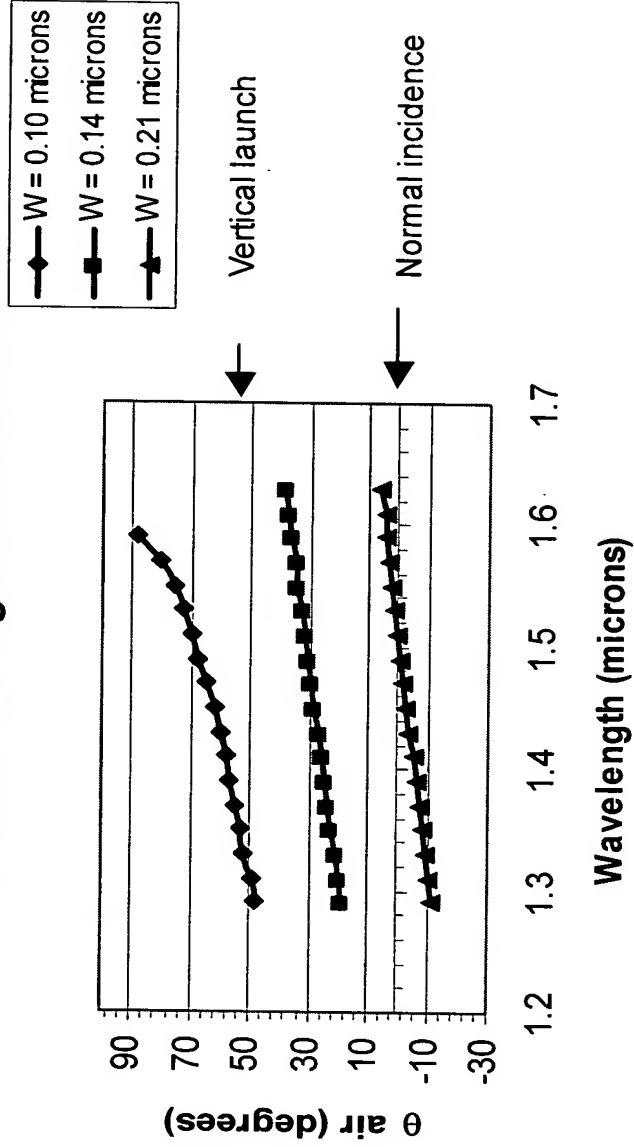


FIG. 4.

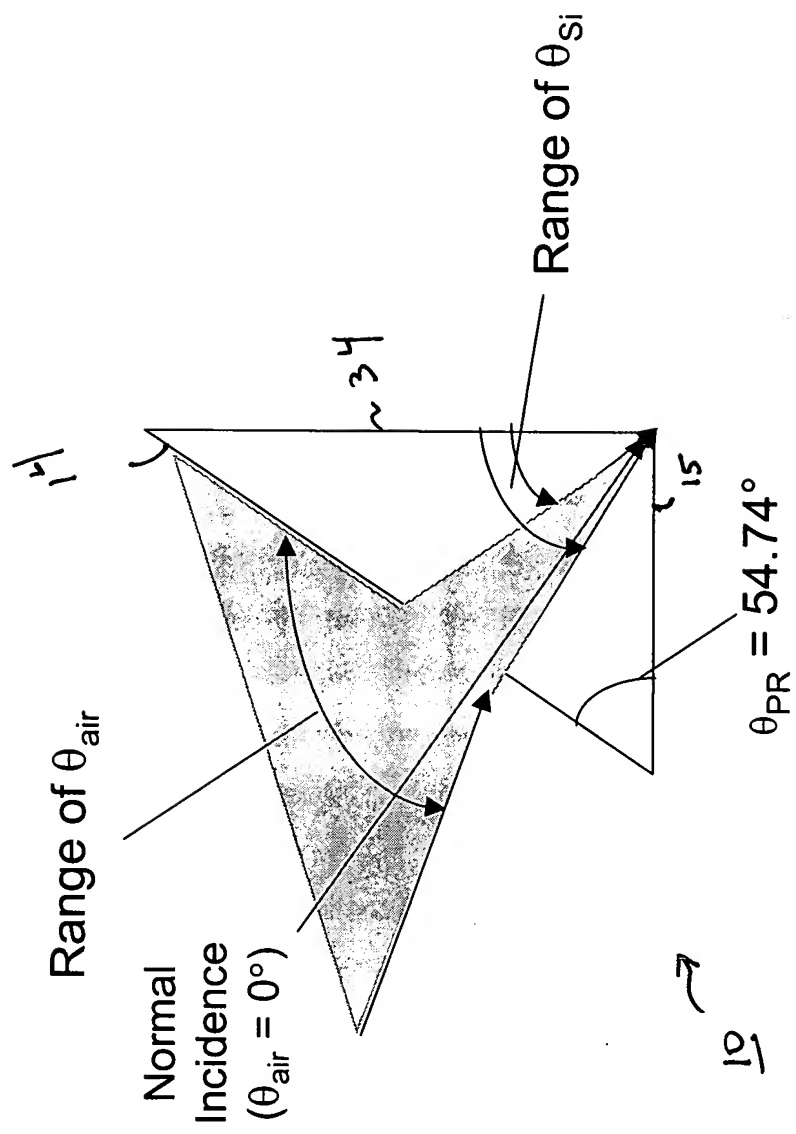


FIG. 5.

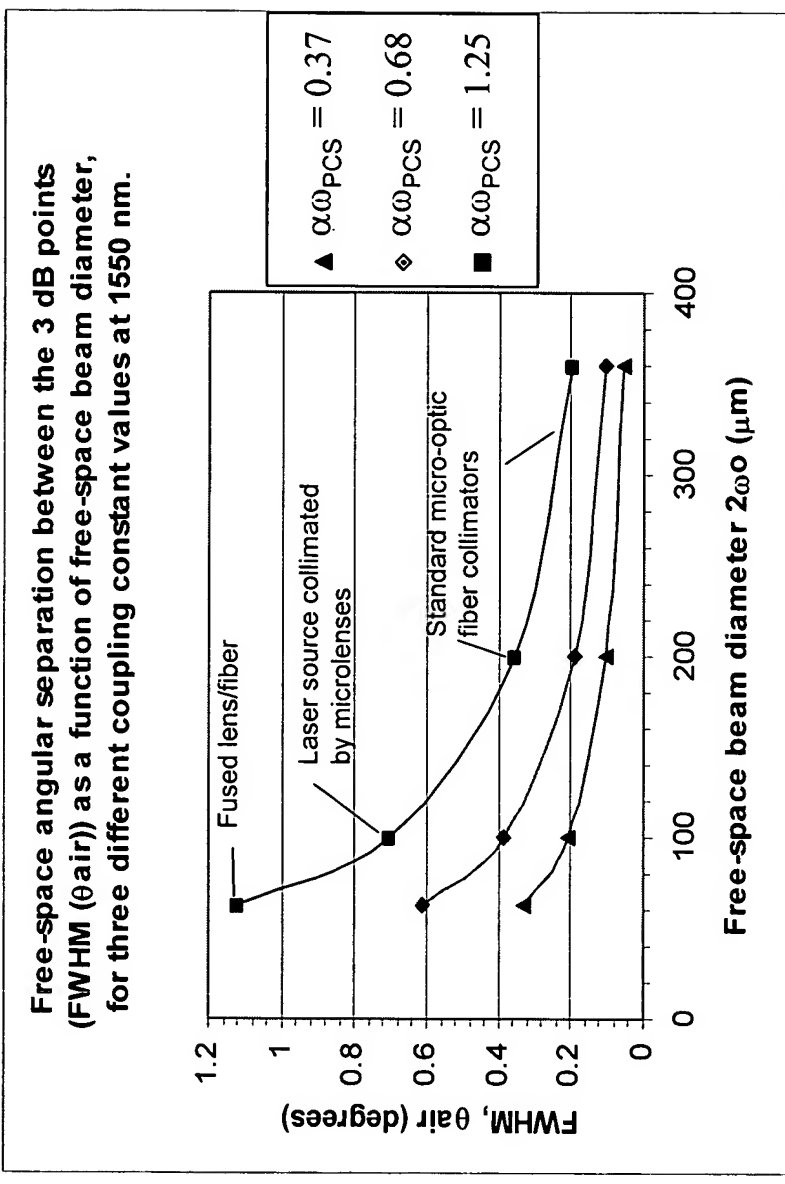


FIG. 6.

$n = 1.45$ for evanescent layer

Coupling loss vs "constant" silicon dioxide ($n = 1.45$)
evanescent coupling layer thickness, $\lambda = 1550$ nm, $2\omega_0 = 63$
 μm in air, as a function of waveguide thickness

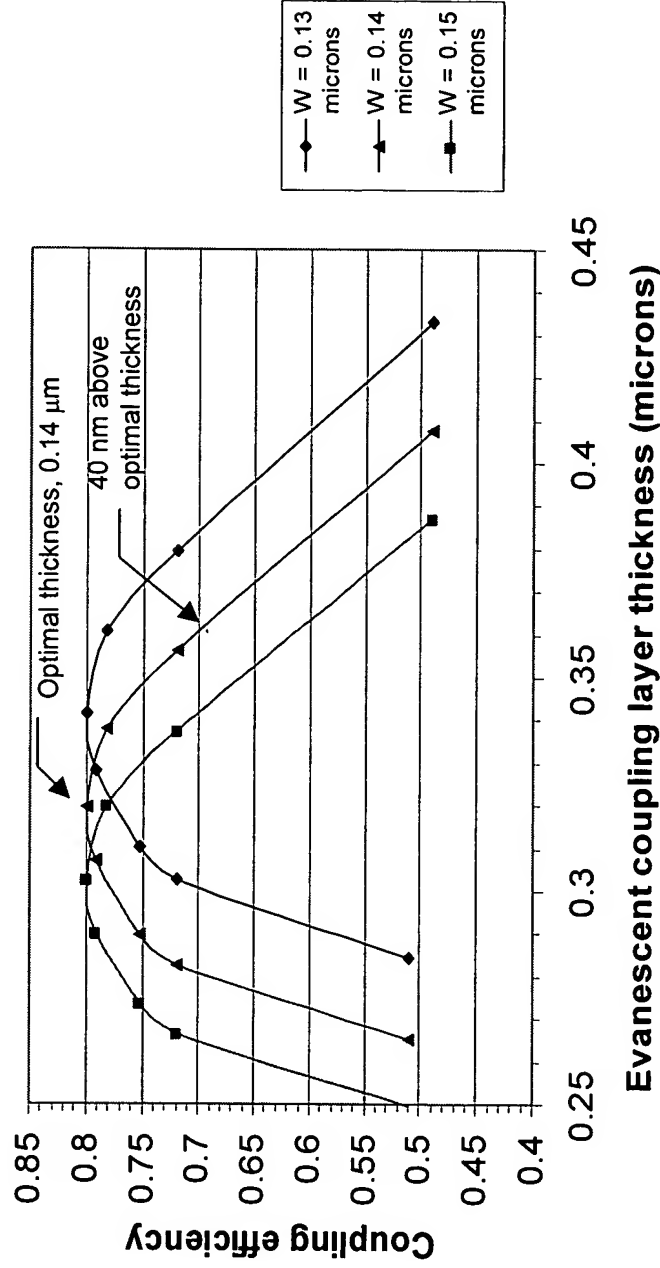


FIG. 7.

Coupling efficiency vs. evanescent coupling layer thickness,
 $\lambda = 1550$ nm, $2\omega_0 = 63$ μ m, $W = 0.14$ μ m, for three different
refractive index values of the evanescent coupling layer.

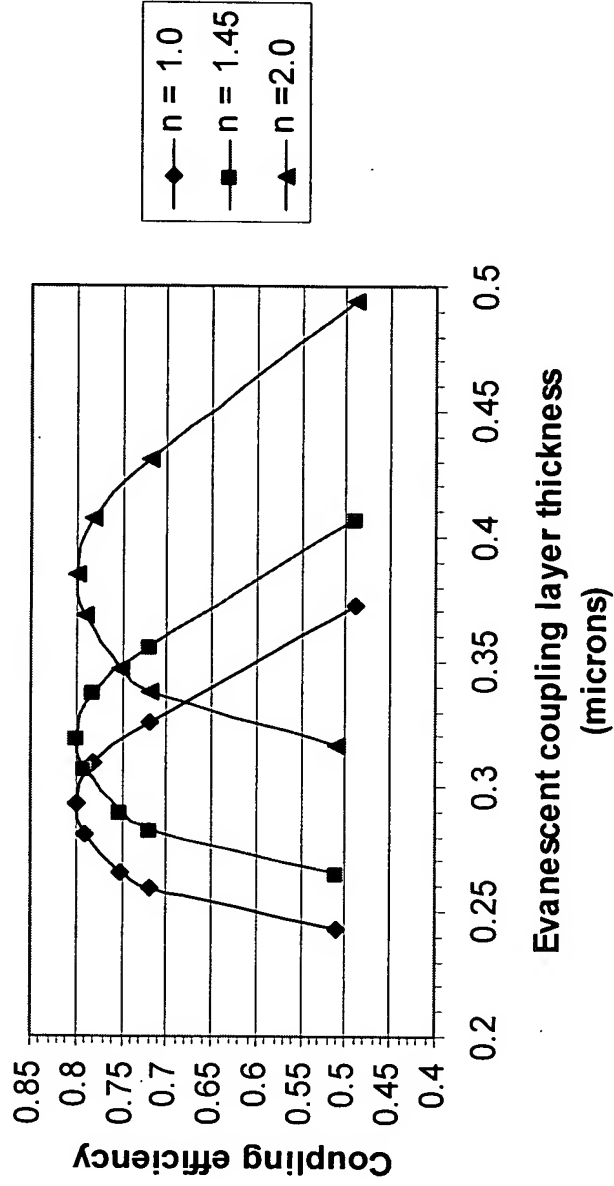


FIG. 8.

STO-0107
9/22

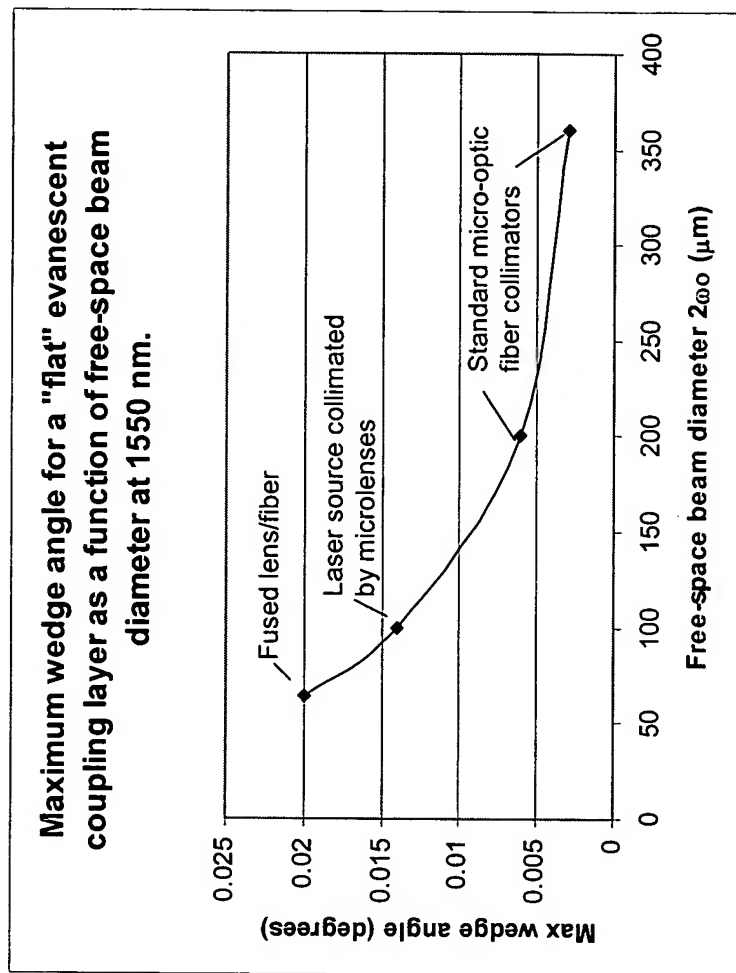


FIG. 9.

Optimum wedge angle for a tapered evanescent coupling layer (linearly varying in thickness) as a function of free-space beam diameter at 1550 nm.

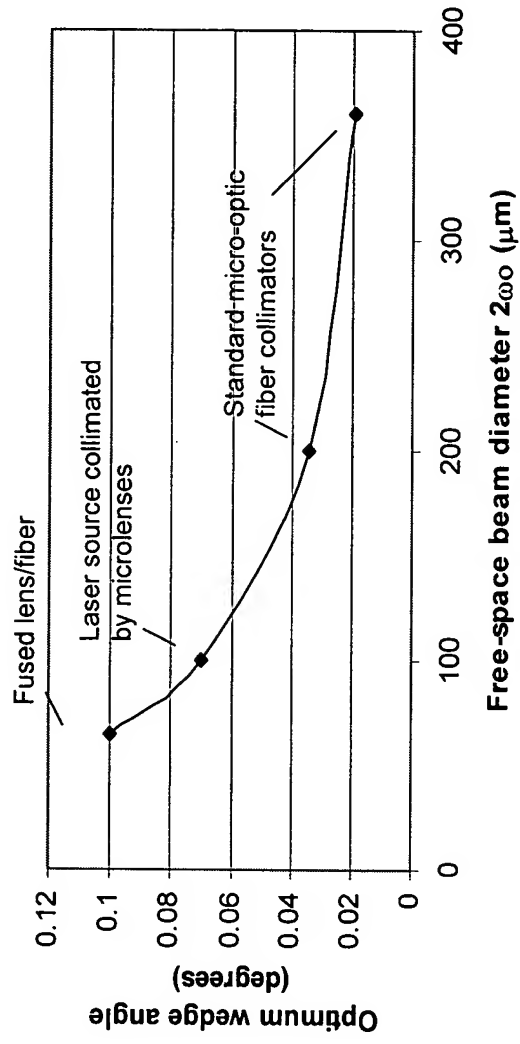


FIG. 10.

Graphs of $2\omega_{PCS}/2\omega_o = \{1 - (\sin\theta_{air}/n_{Si})^2\}^{1/2} / \{\cos\theta_{air} * \cos\theta_{Si}\}$

Ratio of projection of input beam on prism coupling surface to free space beam size, as a function of wavelength for 4 different waveguide thicknesses of the embodiment shown in Figure 2.1, with $\theta_{pr} = 54.74$ degrees.

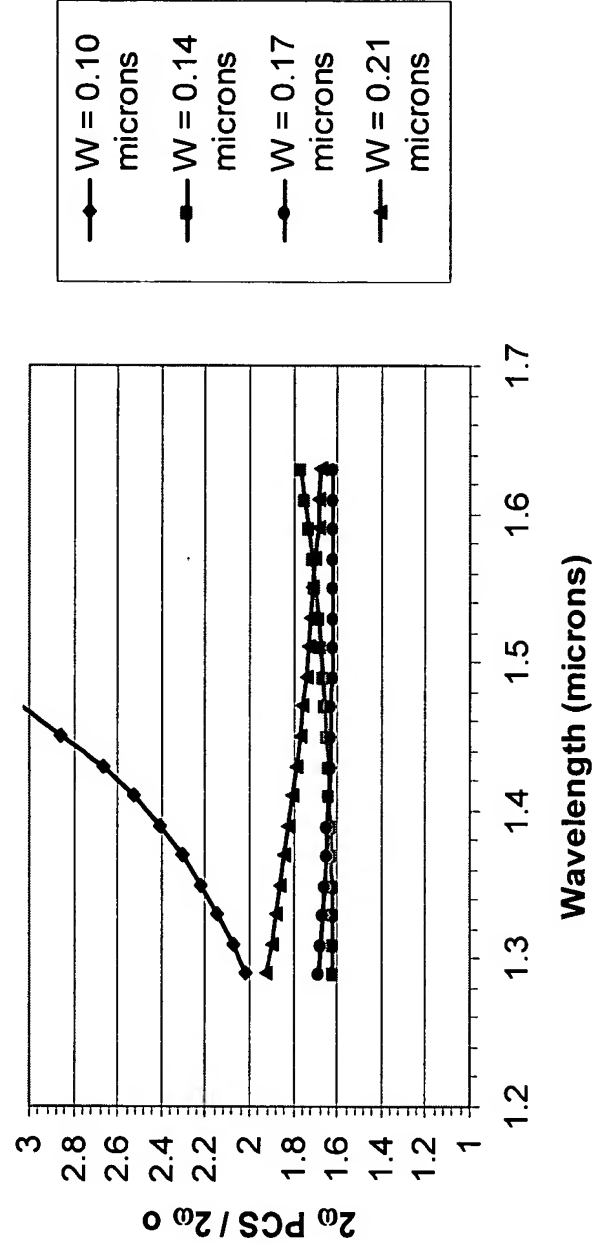


FIG. 11.

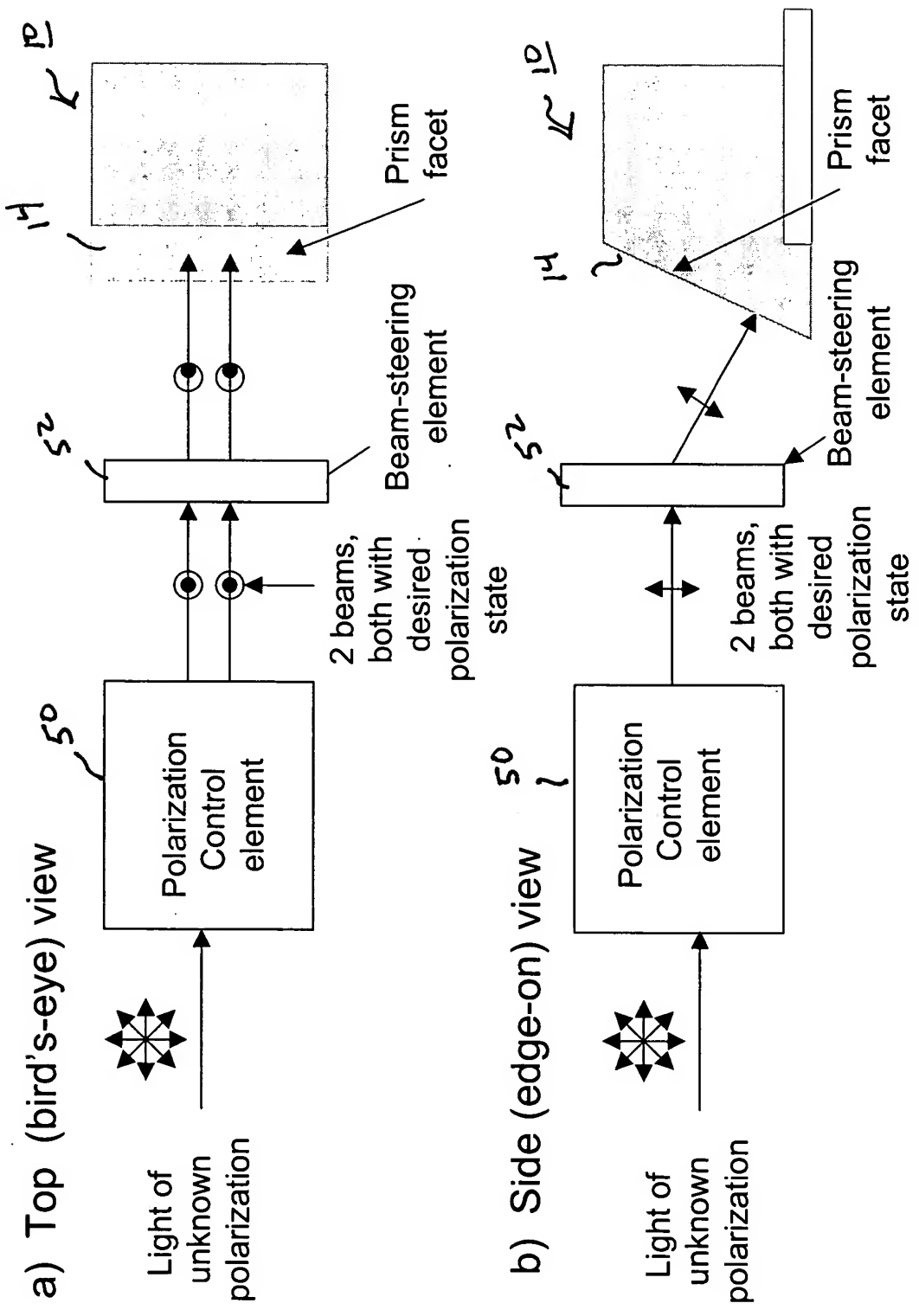


FIG. 12.

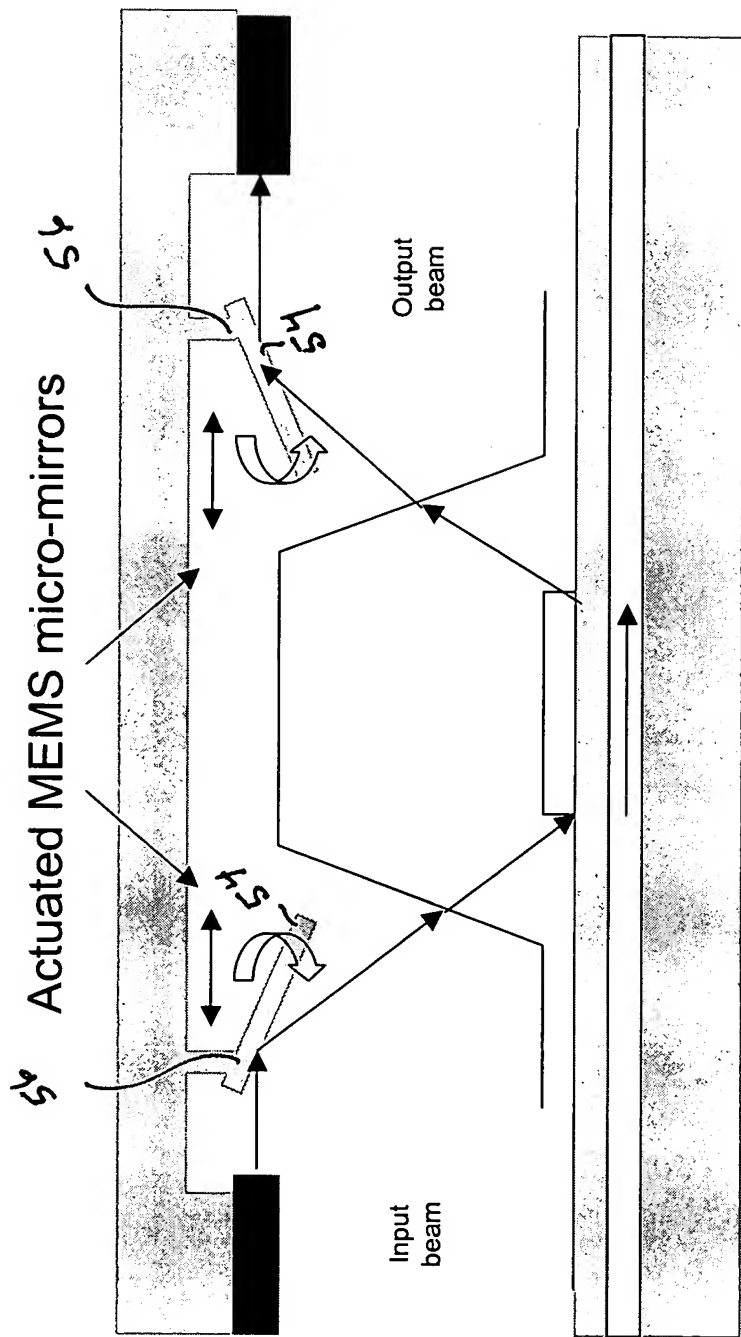


FIG. 13.

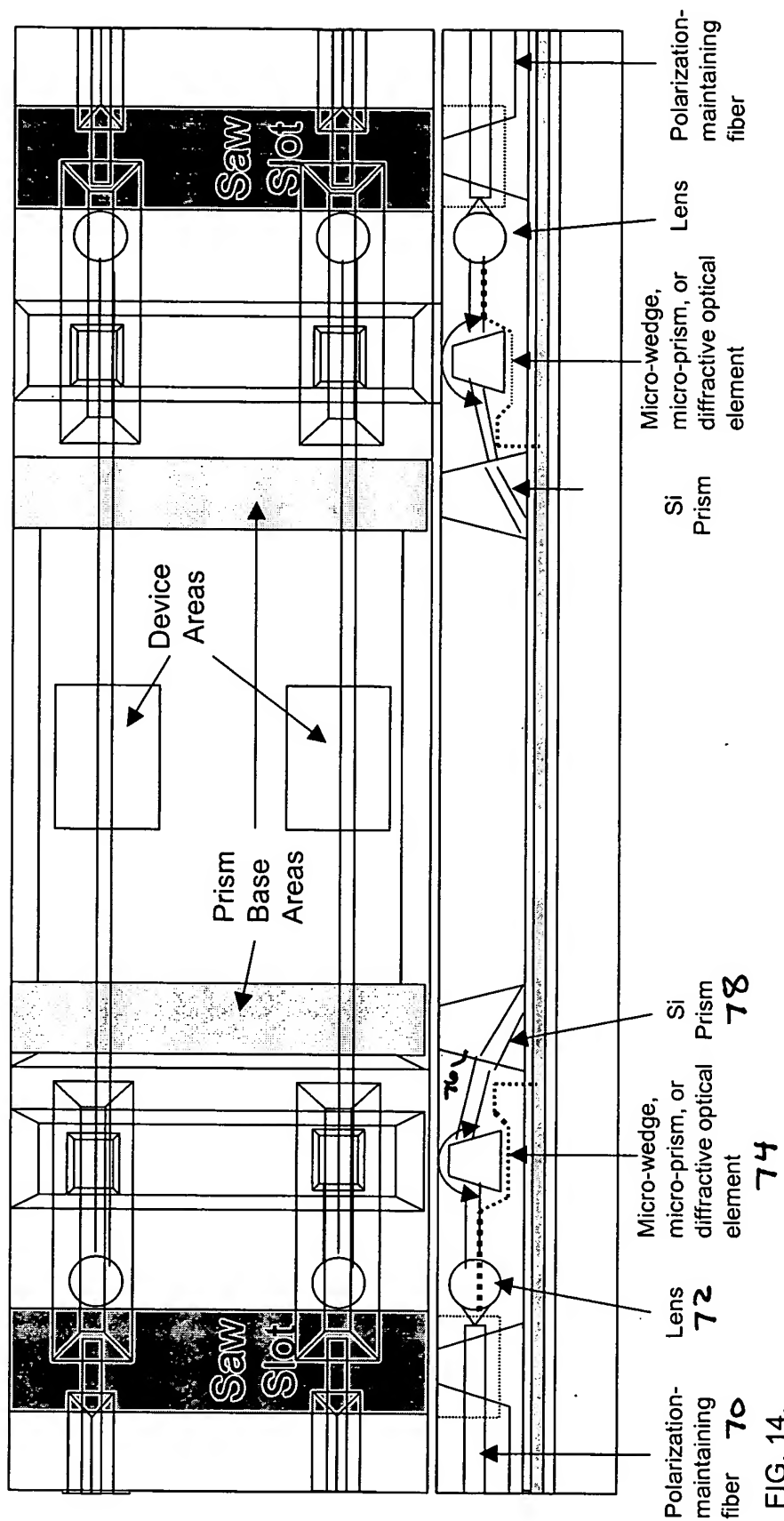


FIG. 14.

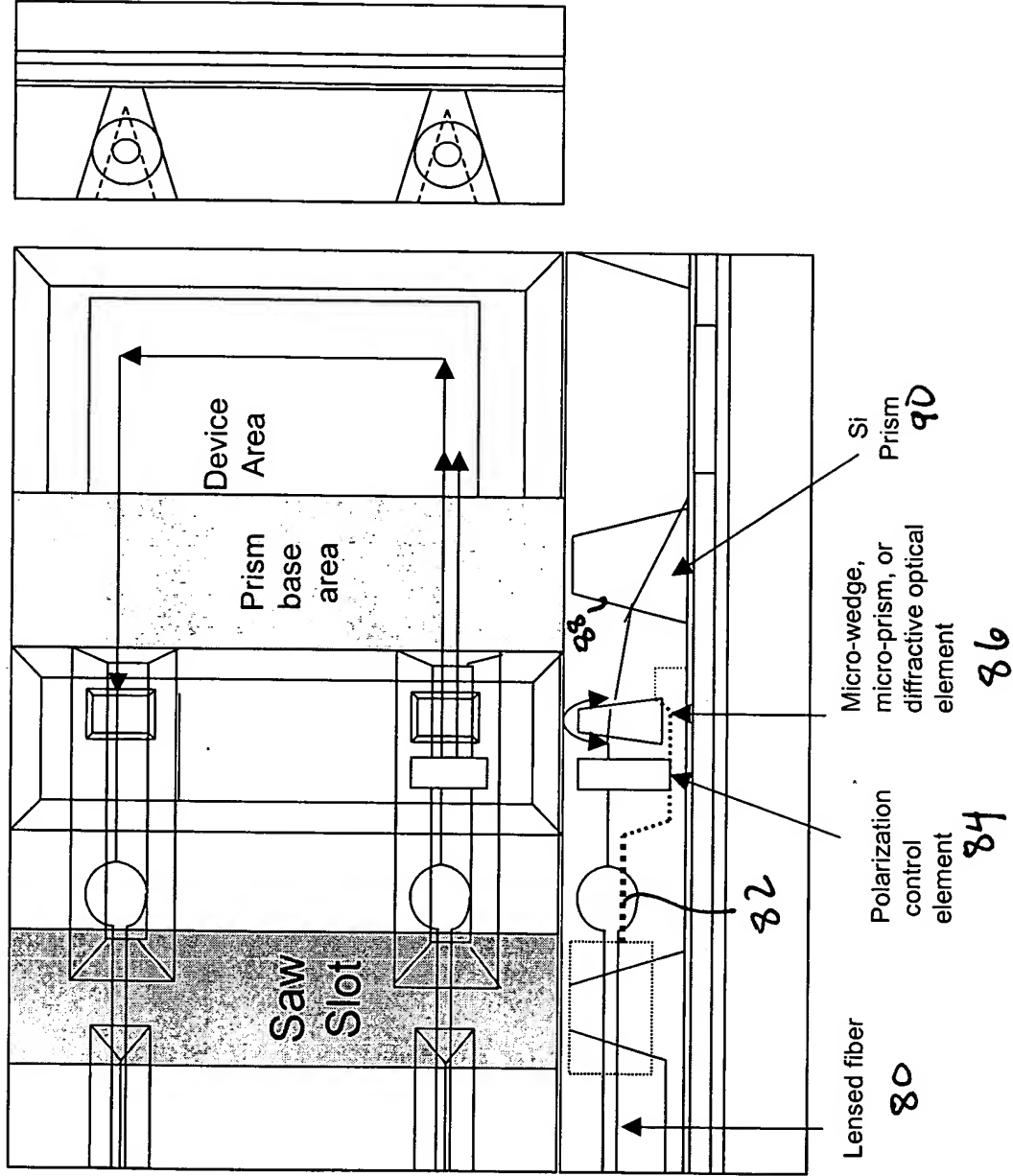


FIG. 15.

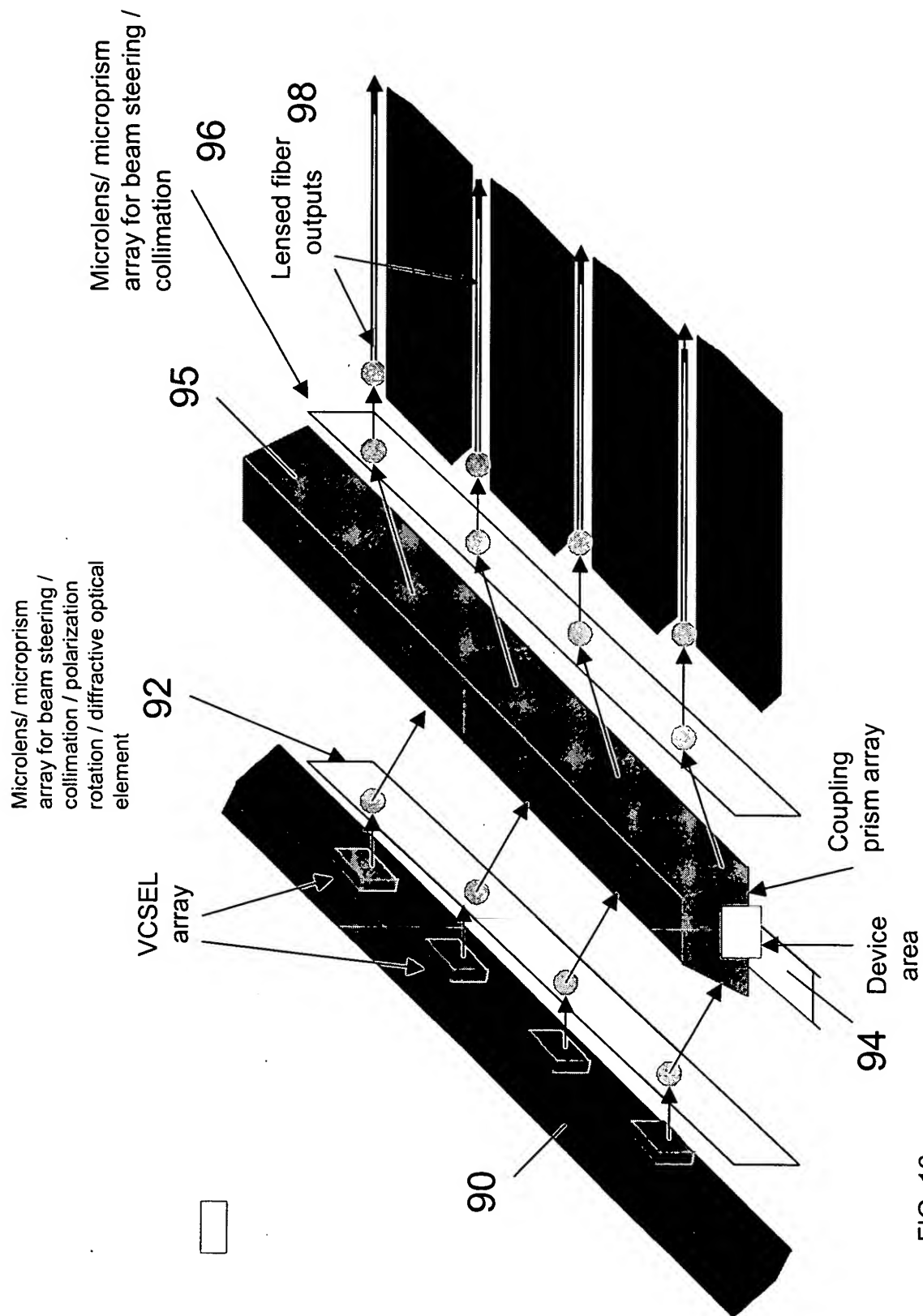


FIG. 16.

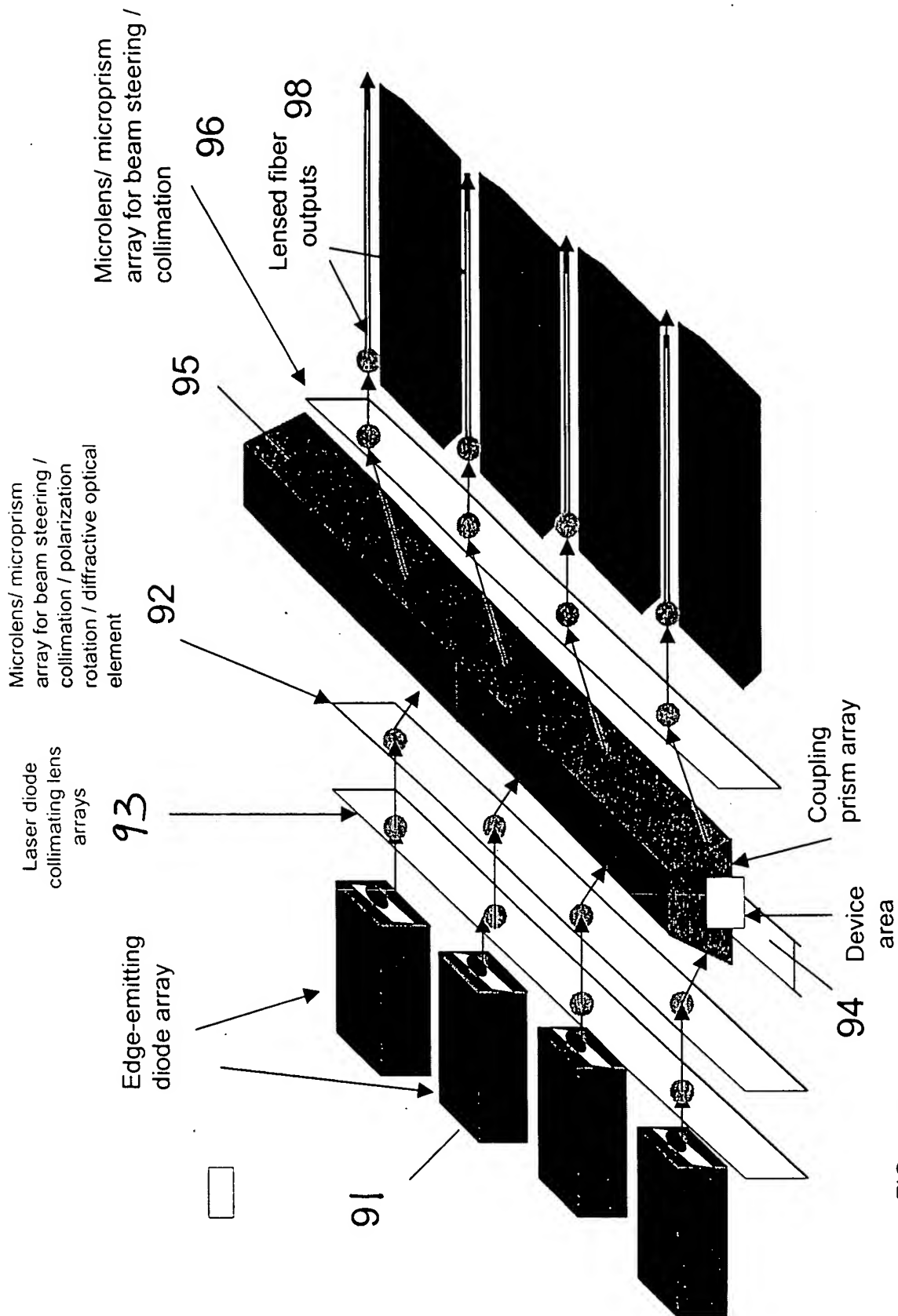


FIG. 17

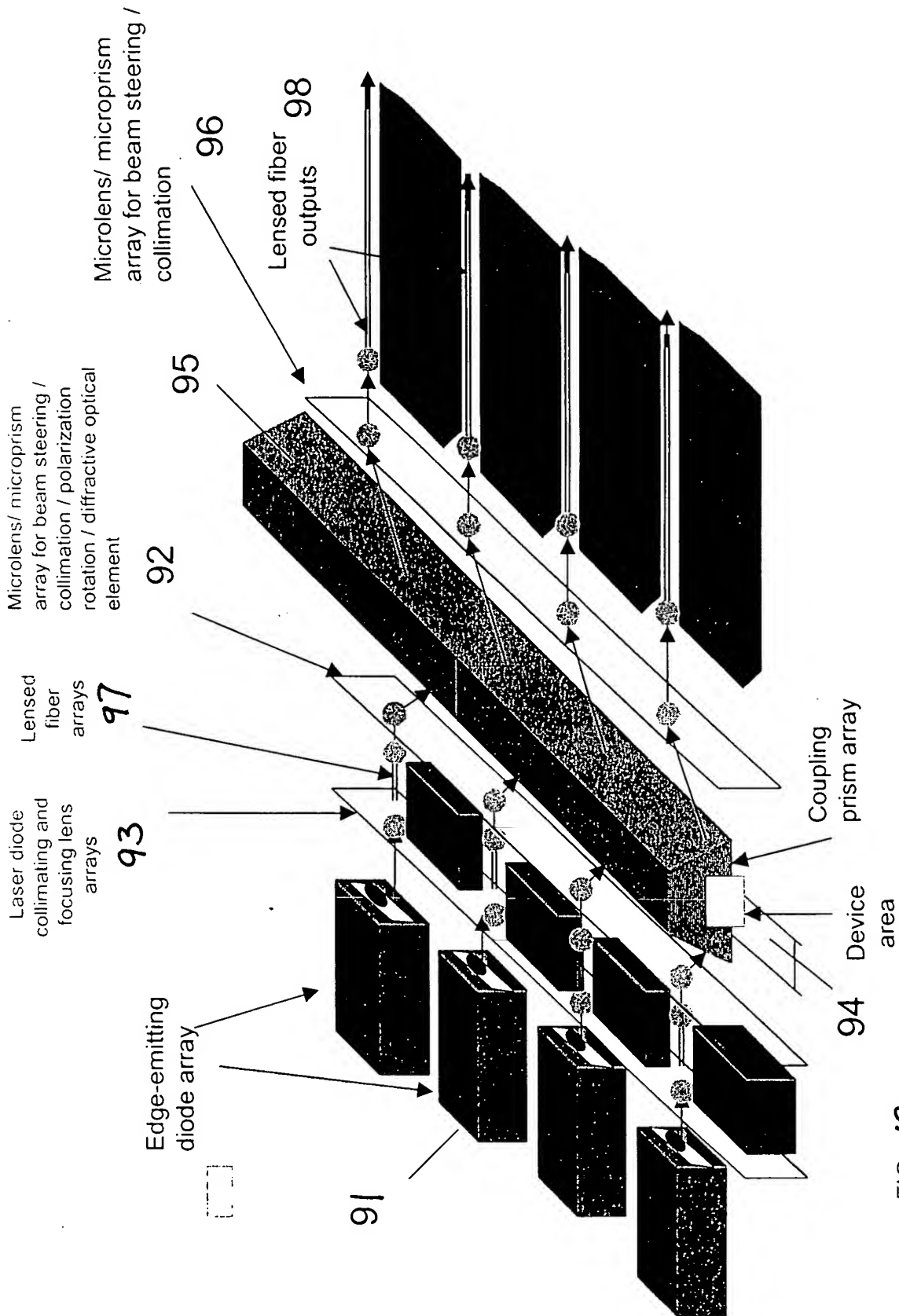


FIG. 18

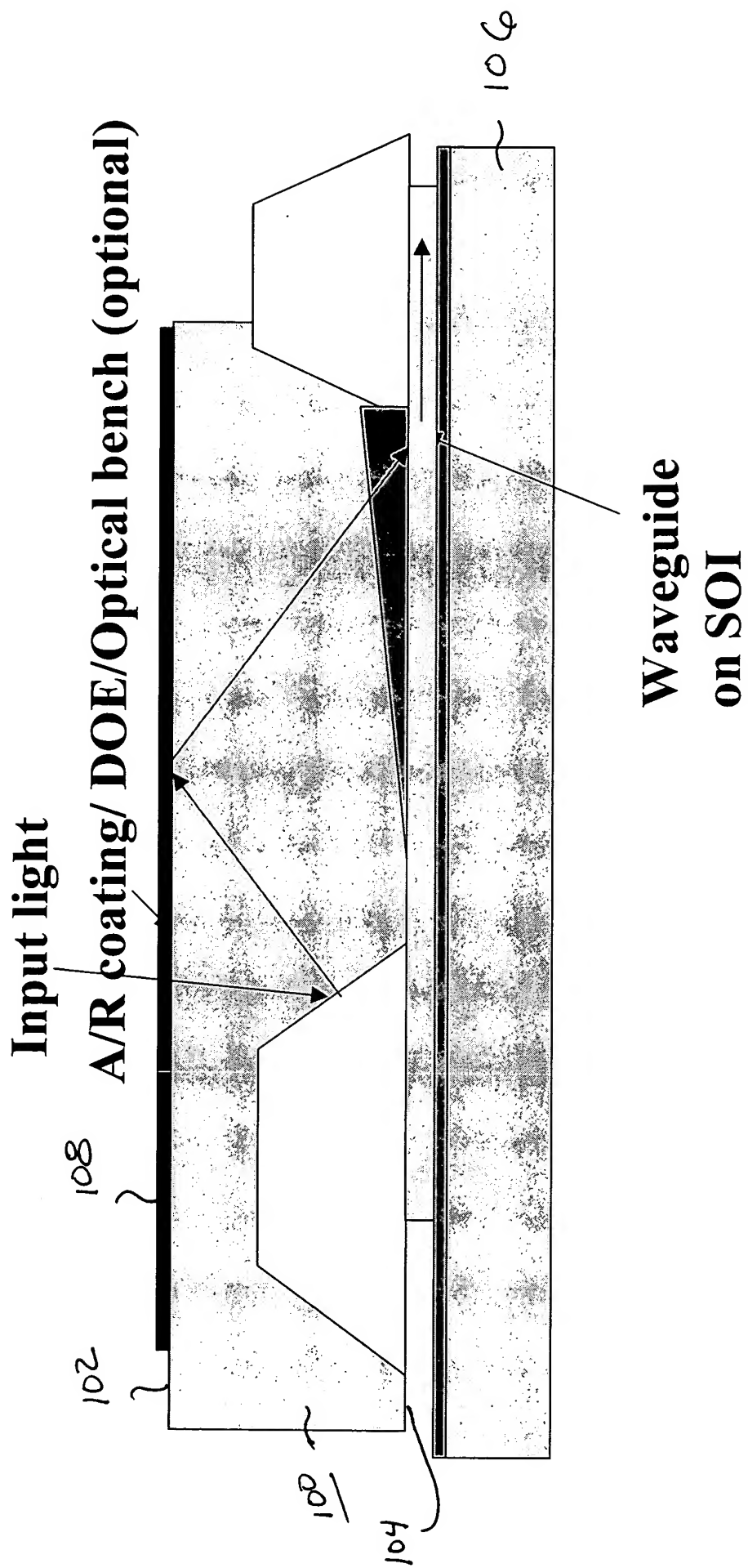


FIG. 19.

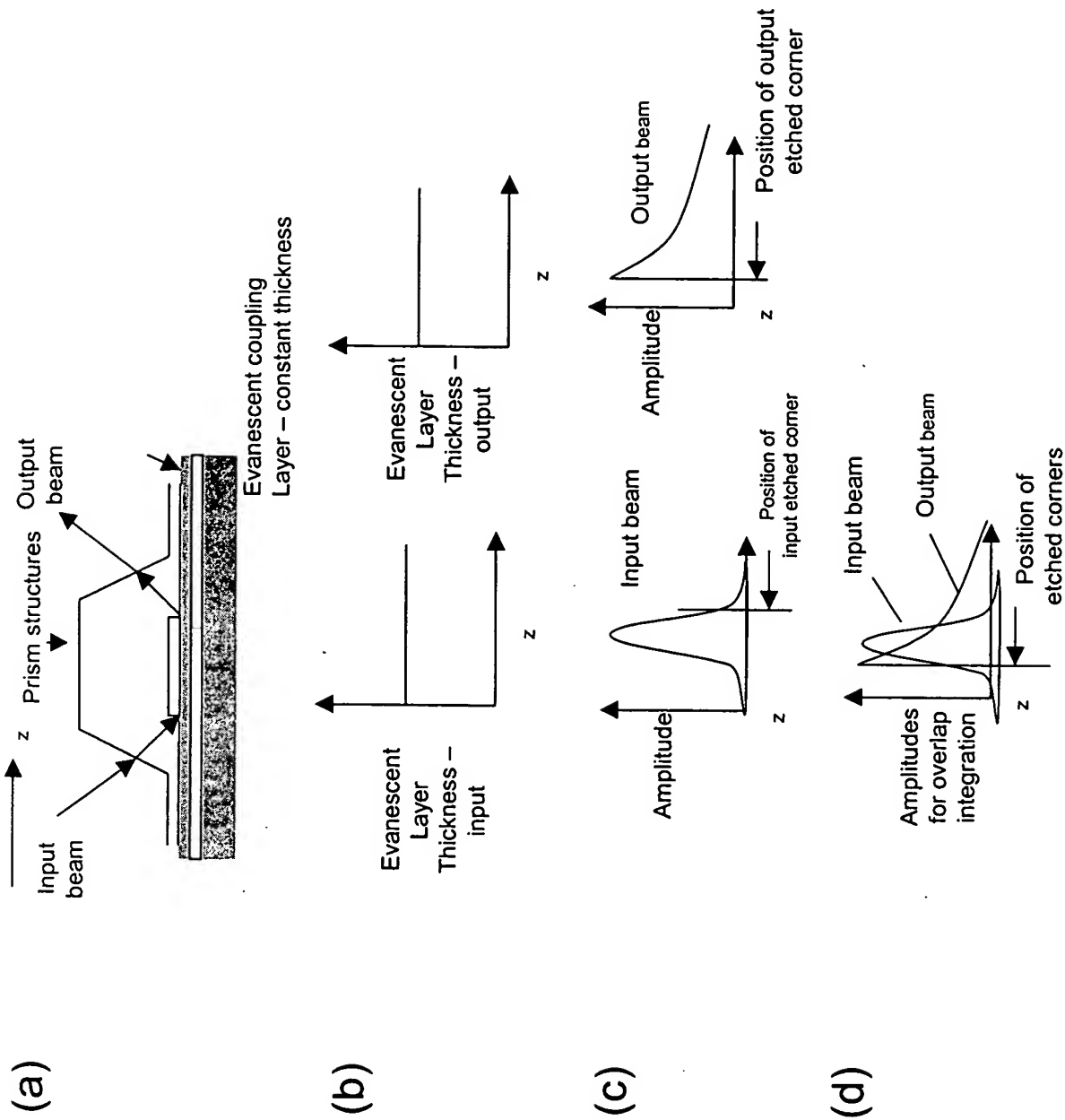


FIG. 20

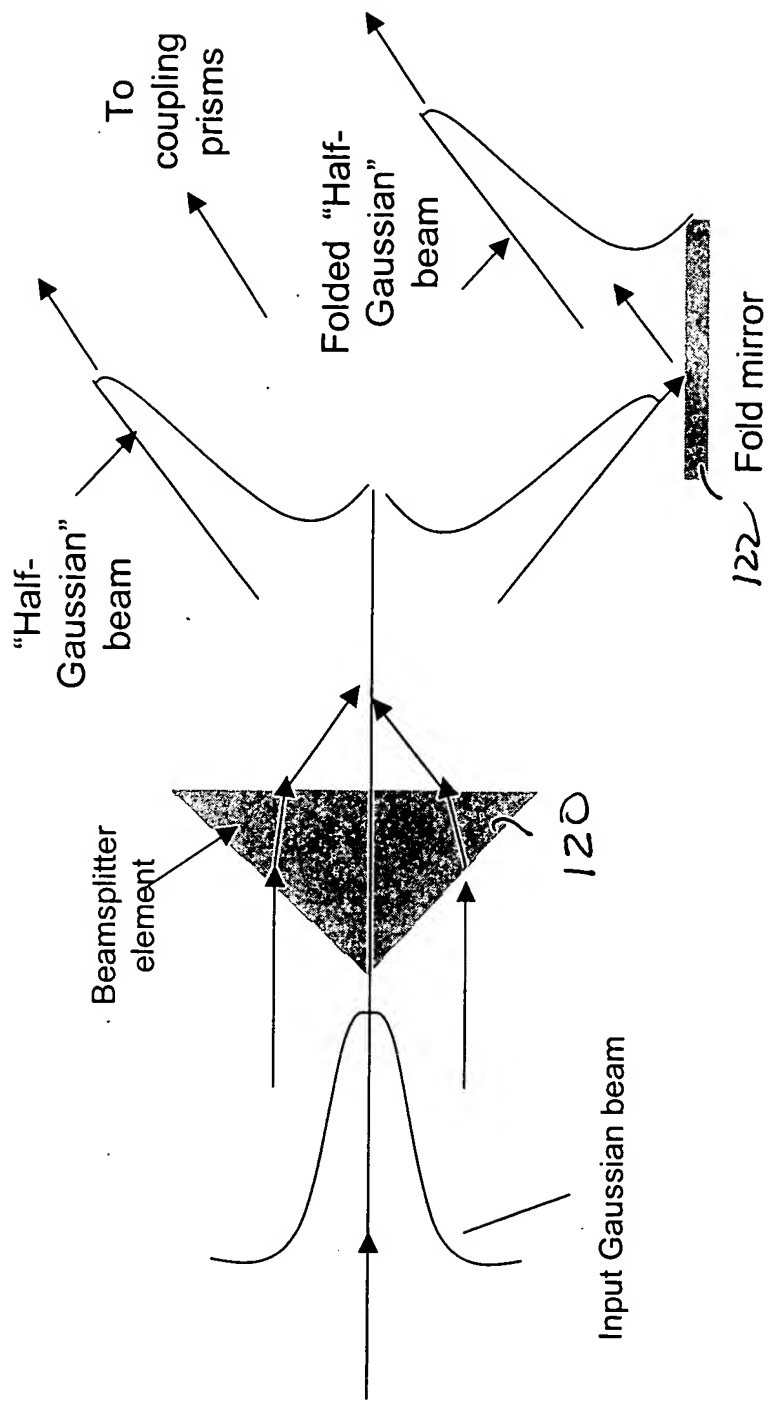


FIG. 21

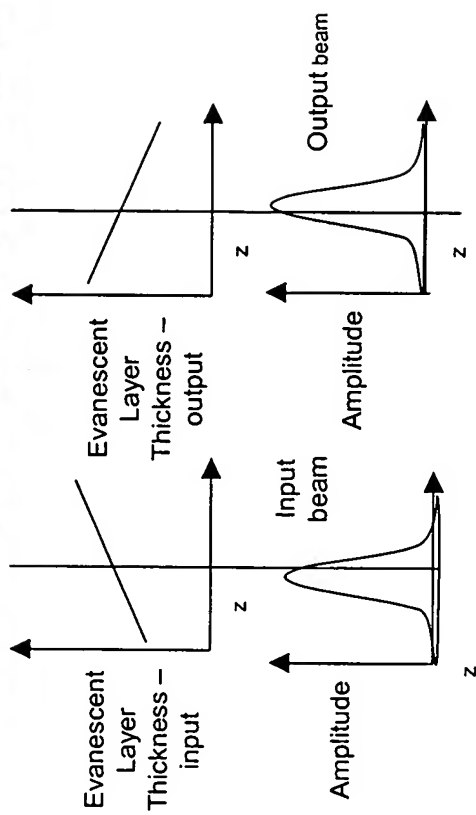
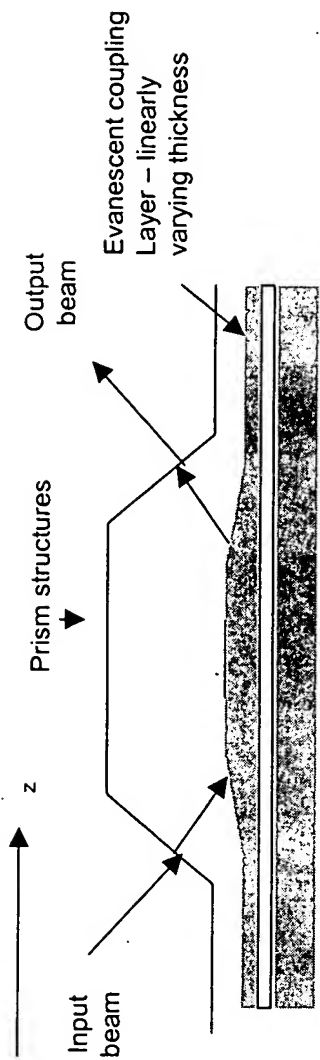


FIG. 22